The ISO-SWS detectors: Performance trends and space radiation effects

A. M. Heras, E. Wieprecht *, H. Feuchtgruber †, F. Lahuis ‡,
K. Leech, R. Lorente, P. Morris §, A. Salama and B. Vandenbussche ¶
ISO Science Operations Centre, Astrophysics Division,
Space Science Department of ESA,
Villafranca, P.O. Box 50727, 28080 Madrid, Spain

Abstract. We present a trend analysis of the ISO-SWS detector performance and a study of the space radiation effects on the SWS detectors. In particular, dark currents, dark current noise and detector responses have been checked as a function of time through the mission and as a function of time in a revolution. The results show that these parameters were stable during the mission in all bands but for band 3 (Si:As). Dark currents and responses were found to be higher in the first hours following the start of the science window, especially in band 2 (Si:Ga). We have studied the impacts of cosmic rays and radiation belt particles on the SWS detectors, as well as of the only large solar proton event on November 6, 1997, that occurred during the ISO mission (operated during solar minimum). The observed glitch rates in all SWS bands are found to be between 2 and 4 times higher than the value predicted by the CREME96 model for the cosmic ray flux in the period considered. The bands that registered the highest glitch rates showed also a correlation with the electron fluxes measured on the GOES 9 spacecraft. From the distribution of glitch heights (voltage jumps in the detector signal), we have derived the deposited energy distributions of the particles hits. Our results lead to the conclusion that secondary particles produced in the shield and the detectors contributed at least as much as cosmic rays to the observed glitch rate. The effects on the detectors of the November 6, 1997 event, which caused that all observations in a revolution were declared failed, are described in detail.

1. Introduction

The Short Wavelength Spectrometer (SWS) is one of the four instruments on board the Infrared Space Observatory (ISO), which was developed by the Space Research Organization of the Netherlands (SRON) and the Max Planck Institut für Extraterrestrische Physik (MPE). It consists of two grating spectrometers, covering the wavelength range from 2.38 to 45.2 μm with a spectral resolution between 1000 and 2000, that is increased to 30,000 by inserting Fabry-Pérot filters. The

* also Max-Planck Institut für Extraterrestrische Physik, Garching, Germany
† also Max-Planck Institut für Extraterrestrische Physik, Garching, Germany
‡ also SRON, Groningen, The Netherlands
§ also SRON, Utrecht, The Netherlands
¶ also Instituut voor Sterrenkunde, University of Leuven, Belgium

© 1998 *Kluwer Academic Publishers. Printed in the Netherlands.*

output of each grating spectrometer is re-imaged onto two detector arrays of 12 elements each. The FP output is directed to one of the FP arrays (two detectors each). An overview of the characteristics of the detector arrays is given in Table I. For a more detailed description of the instrument see de Graauw *et al.* (1996).

ISO was launched on November 17, 1995 into a highly elliptical orbit of a 24 hours period, with the perigee and the apogee located at 1000 km and 70,600 km, respectively. Around perigee passage the instruments were switched off to avoid radiation damage induced by the proton belts. The instrument activation window was open between 1h 55m and 3h 20m after perigee, when the satellite altitude was around 26500 km. The scientific observations window started 4 hours after perigee passage, at an altitude of 43214 km, and had a duration of 16h 56m with a short interruption of 15 m, for the antenna handover between the ESA VILSPA and NASA Goldstone ground stations. ISO's liquid Helium was depleted on April 8, 1998, after ISO had been operational during 875 revolutions.

Detector dark currents and responses to internal stimulators were systematically checked throughout the mission, both in dedicated calibration observations and in each astronomical observation. Dark current measurements were carried out by closing the instrument shutter and checking the current levels in each detector. Four different internal calibration sources, each with two intensity levels, were built-in to check the detector response. In particular, the grating calibrator source in low state was used as a photometric check in each astronomical observation. Band 1 response to the grating calibrator source, set low, was not high enough to be measured, but due to the band stability and good behaviour these checks were not necessary in every observation. This was confirmed by calibration observations in which the grating calibrator

Table I. SWS Detector arrays

Array	Detector type	Number of pixels	Wavelength range (μm)
Band 1	InSb	12	2.38 - 4.1
Band 2	Si:Ga	12	4.1 - 12
Band 3	Si:As	12	12 - 29.5
Band 4	Ge:Be	12	29.5 - 45.2
Band 5	Si:Sb	2	11 - 26
Band 6	Ge:Be	2	26 - 45

source was set to high, and by the reproducibility of the astronomical standard sources observations.

In the first section of this paper we describe the long term behaviour of the SWS detectors, analyzing dark currents, dark current noise and responsivity trends as a function of time in the mission and as a function of time in the revolution (i.e., position in orbit). In the second part we study the impact rates of cosmic rays and radiation belt particles on the SWS detectors and we discuss their relation with the space weather and the nature of the particles responsible for the impacts.

2. Trend Analysis

The behaviour of the SWS detectors has been closely monitored during ISO's lifetime. The trend analysis of these parameters has been carried out for operational purposes, but the results obtained are also relevant to other missions in which the same type of detector materials will be used. In particular, detector dark currents, dark current noise and detector response to internal calibrator sources have been used to check the detector status. The variation of these characteristics has been studied (1) as a function of time in the mission, to analyze long term trends, and (2) as a function of time in the revolution, to check for systematic variations depending on the elapsed time after the instrument has been switched on and the position of the satellite in orbit.

2.1. Data

The long term trend study has been based on the internal-check calibration observations and the dark currents measured at the end of the SWS activation sequence. The internal-check calibration observation measured the dark currents, the response to the diffuse calibrator, set low, and the response to the grating calibrator, set low (scanning and at fix grating position), each measurement lasting five minutes. This observation was executed in the ISO calibration revolution once a week. It was normally scheduled as the first observation after the science observation window had been opened, or around apogee when that was not possible. As a daily check, dark currents were also routinely measured for two minutes at the end of the SWS activation sequence. In both observations, the setting of the dark currents was gain 16x and reset time interval 2 seconds.

The behaviour of the SWS detectors as a function of time in the revolution has been analyzed using the dark currents and photometric checks (grating calibrator source, set low) measured in every astro-

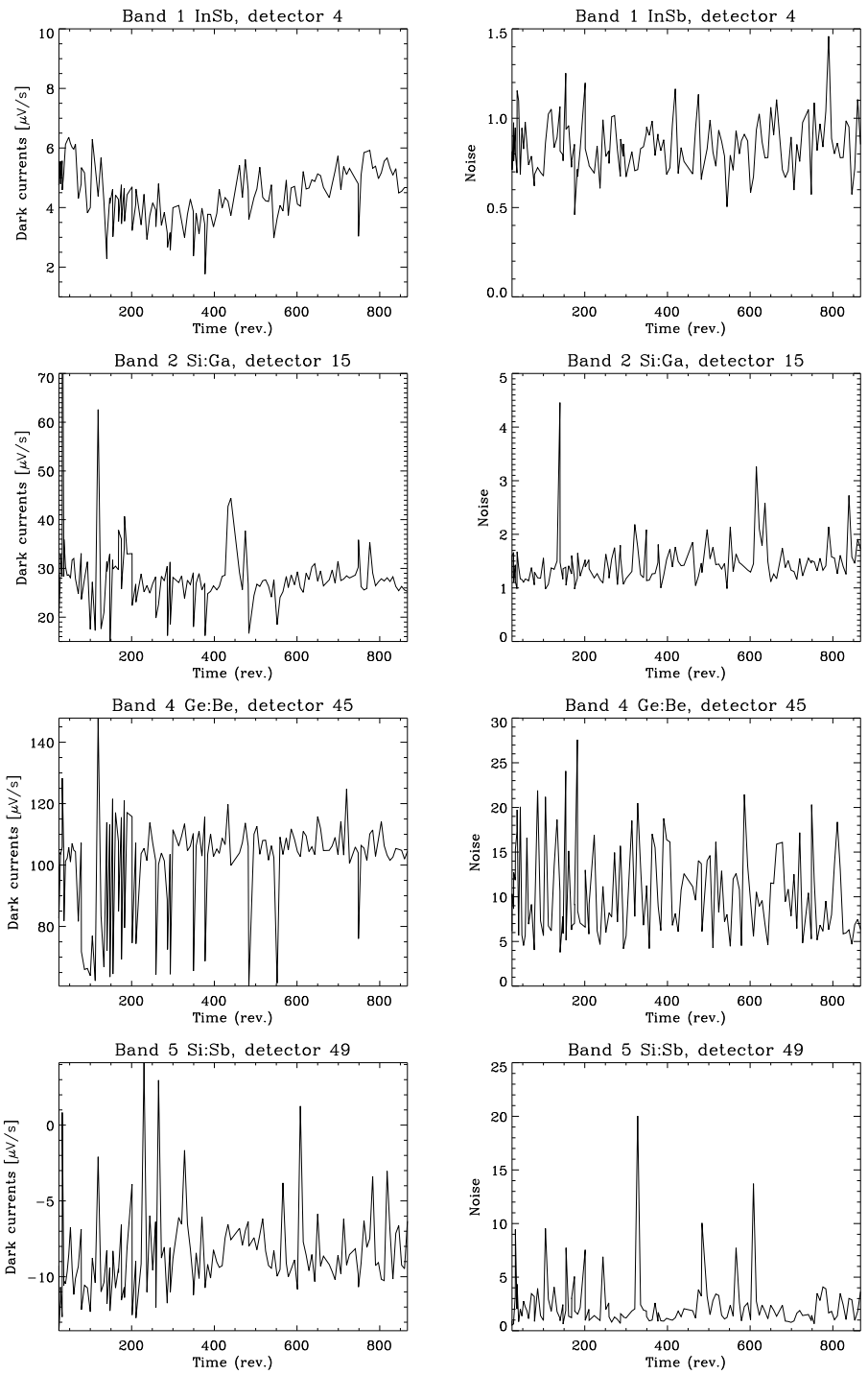

Figure 1. Temporal evolution of dark currents and dark current noise as a function of ISO revolution number for detector bands 1, 2, 4 and 5.

nomical observation. As part of the data off-line processing, the corresponding average values and standard deviations for each detector and observation have been calculated and stored in trend tables accessible through the ISO archive.

2.2. Results

2.2.1. *Long Term Performance*

Figure 1 shows the dark current and dark current noise evolution for five detectors, representative of five SWS detector bands. As can be seen, there are no trends in the dark currents or the noise in bands 1, 2, 4 and 5. The lower peaks in bands 2 and 4 correspond to observations carried out when the satellite was around apogee (this point will be addressed in the next section). The peak in revolution 433 is related to an increase in the OSS (Optical Support Structure) SWS temperature of more than 0.5 degrees, due to a test performed by LWS (Long Wavelength Spectrometer) just before an SWS observation. With regard to band 3, the situation is rather different. Figures 2 and 3 show dark currents and dark current noise, respectively, for all detectors in this band. In most detectors dark currents increase with time, in some cases gradually and in others with a sudden jump in the dark current level. For example, detector 36 dark currents became suddenly ten times higher and after approximately 250 revolutions they decreased abruptly to a fifth of their value. During most of the mission, the worst behaving detectors were 30, 31 and 36. Detector 34 was the worst one during the Performance Verification phase, but after the band 3 bias was set to a lower value in revolution 78, it was rather stable. The peaks that can be seen in all detectors in revolution 93 and 286 correspond to observations in which the bias was temporarily set to a higher level. The peak in the noise in revolution 524 was related to a sudden and simultaneous signal increase in all detectors, followed by a slow decrease. These jumps were relatively frequent and although the cause is not completely understood, they may have been related to particle hits in the instrument electronics. Another characteristic of the dark currents in band 3 detectors is the "pop-corn" noise, or alternate jumps of the dark current between two levels. According to the analysis of the internal-check calibration observations, there is a correlation between the increase of the dark currents and the frequency of observations in which the pop-corn noise dominates. The dark current noise in band 3 detectors does not follow the same trend as the dark currents. Actually, an increase in the noise only appears when the dark currents reach a certain level, as can be seen for detector 36 and in some revolutions in detectors 27, 30 and 31. Summarizing, although the performance of

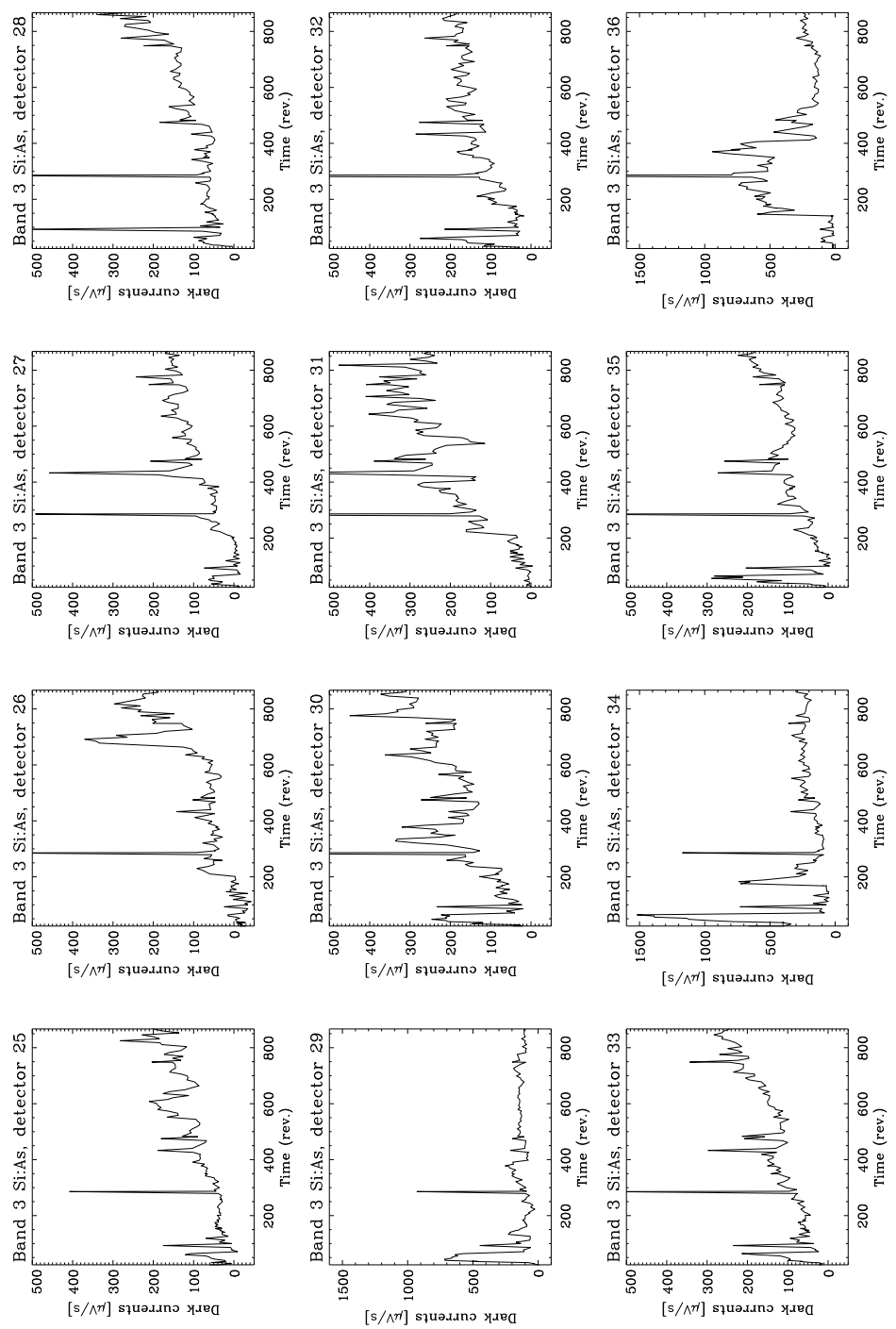

Figure 2. Temporal evolution of dark currents as a function of ISO revolution number for detector band 3.

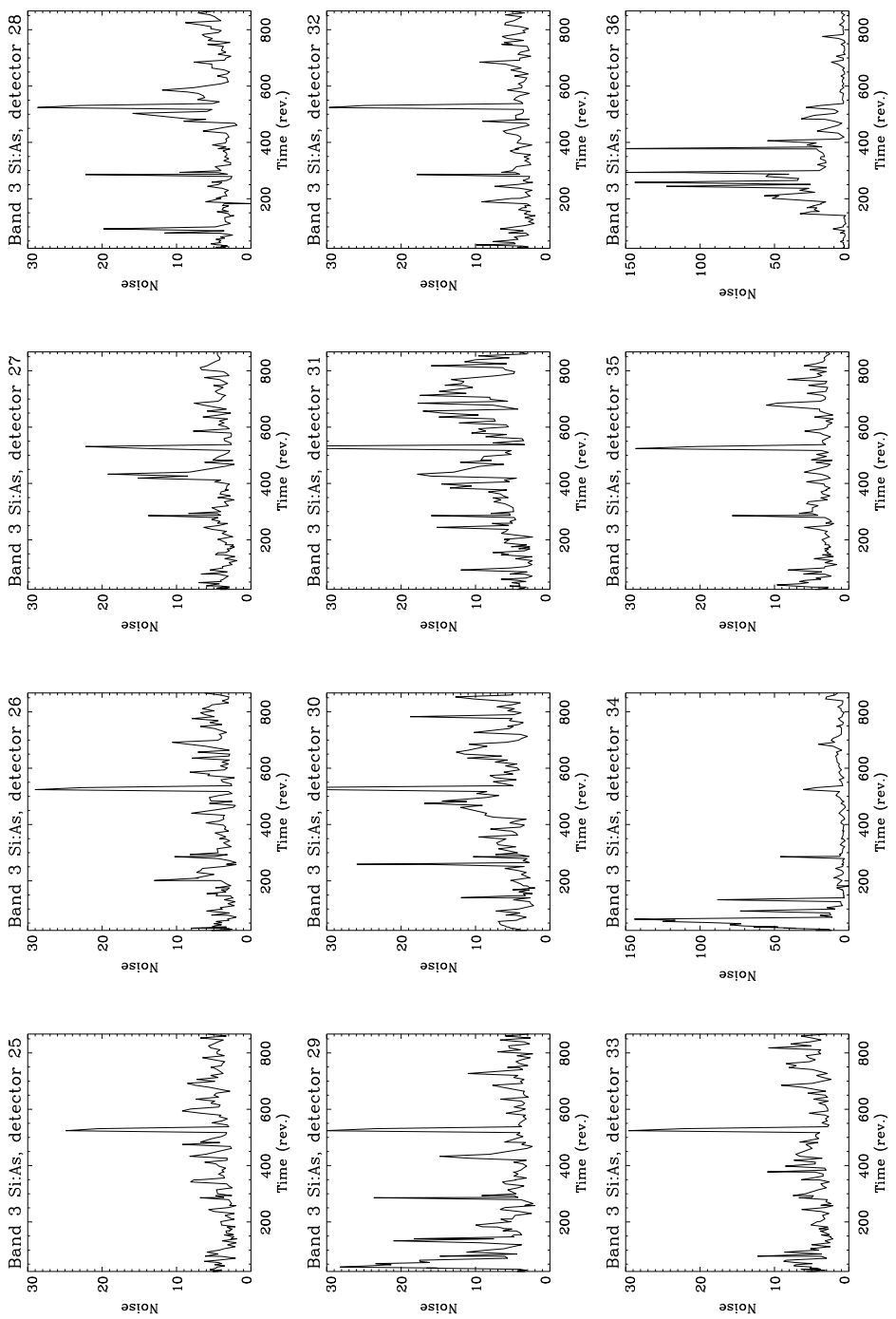

Figure 3. Temporal evolution of dark current noise as a function of ISO revolution number for detector band 3.

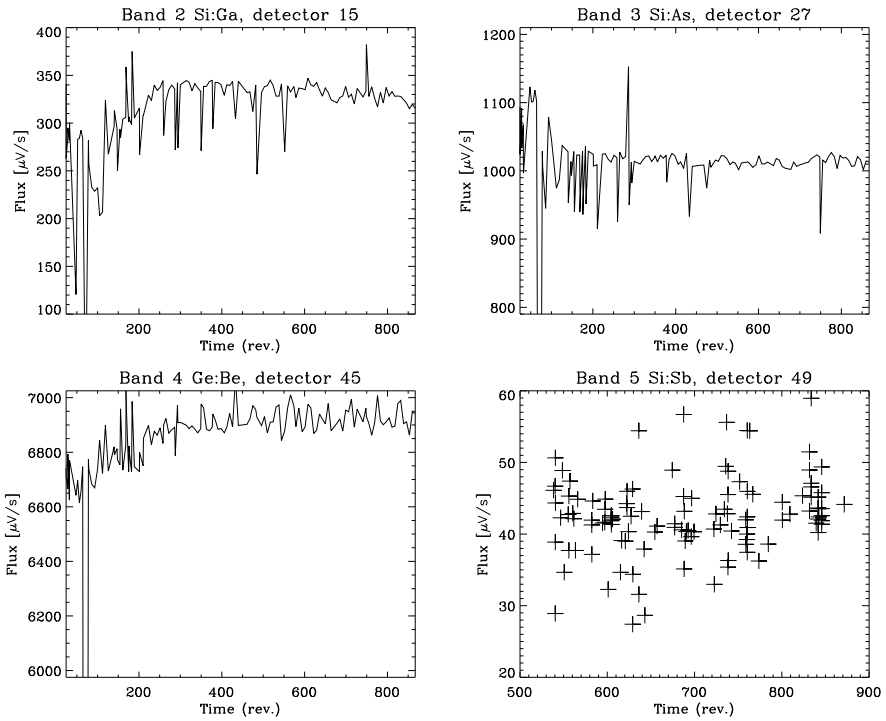

Figure 4. Detector response to the grating calibrator source, set low, as a function of time.

band 3 worsened with time, the process was slow and some detectors showed significant improvements after bad periods, as was the case for detectors 34 and 36. Laboratory tests reproduced successfully the in-orbit behaviour of band 3, by irradiating the Si:As BIBIB detectors with 100 MeV protons (Luinge and Horinga 1997, priv. communication). A 50 rad dose gave already an important increase in dark currents. However, the decrease in dark currents 9 hours after the irradiation that was observed in the laboratory tests, was not seen in orbit. A better curing method that would diminish the radiation damage could not be found.

Long term trends of band 2, 3, 4 and 5 responses to the grating calibrator source were very small, showing variations below 5% (see Figure 4). Band 2 response was rather stable, band 3 response displayed a slight anti-correlation with dark currents in most detectors, and band 4 response increased by a very small amount along the mission. More important response changes were observed depending on the time in the orbit when the measurement was done (see next sub-section).

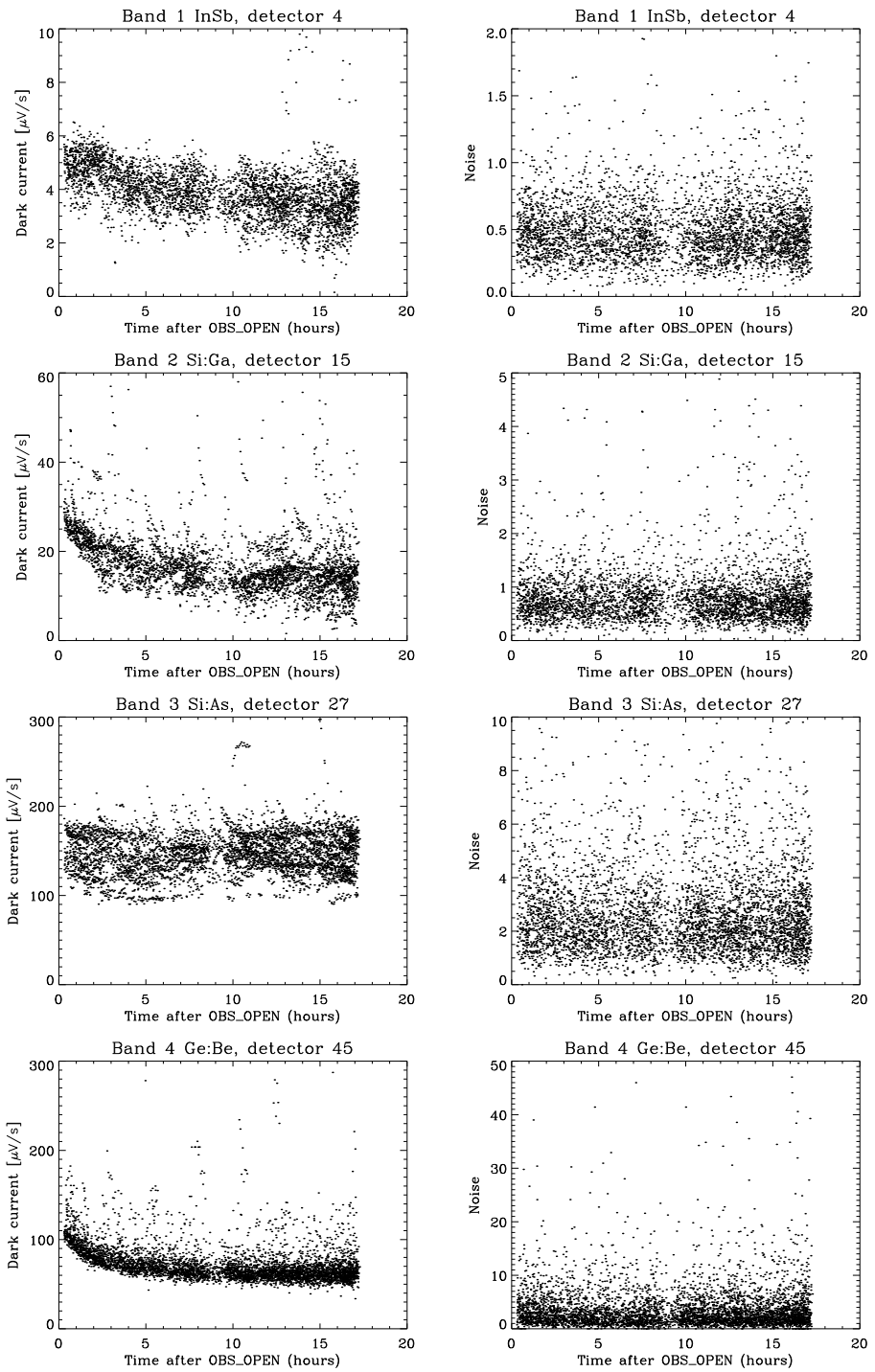

Figure 5. Dark currents and dark current noise as a function of time after the start of the science observation window (or ISO's position in orbit).

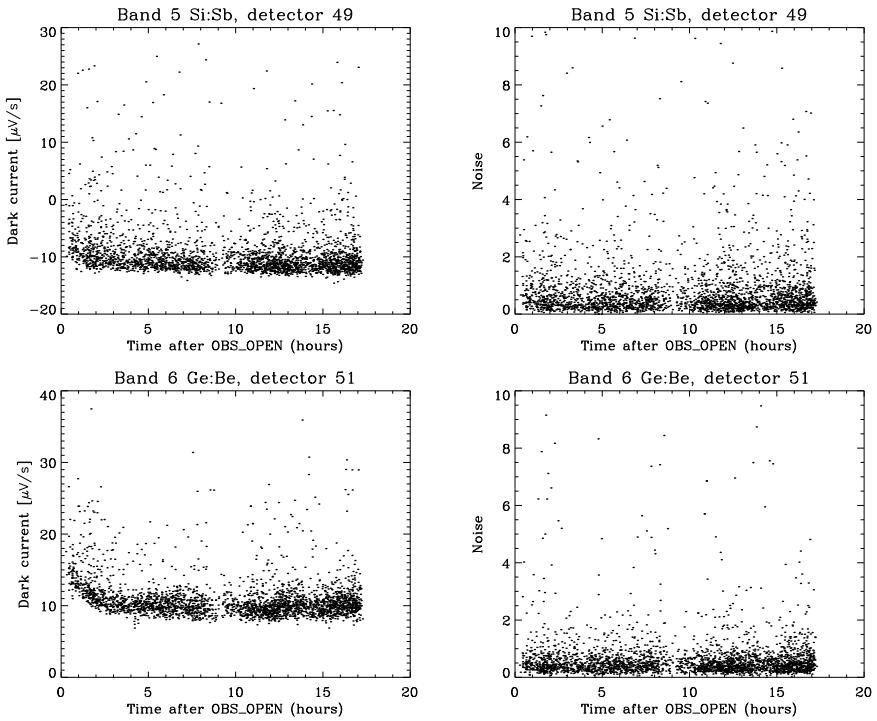

Figure 6. The same as Figure 5 for bands 5 and 6.

2.2.2. *Variation during a Revolution*

In Figures 5 and 6 the evolutions of dark currents and dark noise as a function of time in the revolution are displayed, covering revolutions 537 up to 875. In bands 2, 4 and 6 dark currents were, on average, higher in the first four hours after the start of the science observation window than in the rest of the revolution, by percentages ranging between 15 and 100%. Although also present, the effect was less important in bands 3 and 5, while in band 1 it was only observed in some detectors. On the other hand, as can be seen in the right panels of Figures 5 and 6, the dark current noise did not show any trend, that is, it was constant during the whole revolution. The detector response to the grating calibrator source, set low, as a function of time in the revolution, is shown in Figure 7 for the same interval of revolutions as in Figures 5 and 6. The response of band 2 was, on average, higher in the beginning of the revolution by 40% and decreased linearly until the end. In bands 3 and 4 this behaviour was also observed but below the 10% level. As was mentioned above, the grating calibrator source, set low, was not intense enough to trigger a response in band 1. In order to assess its performance, dedicated observations with the grating

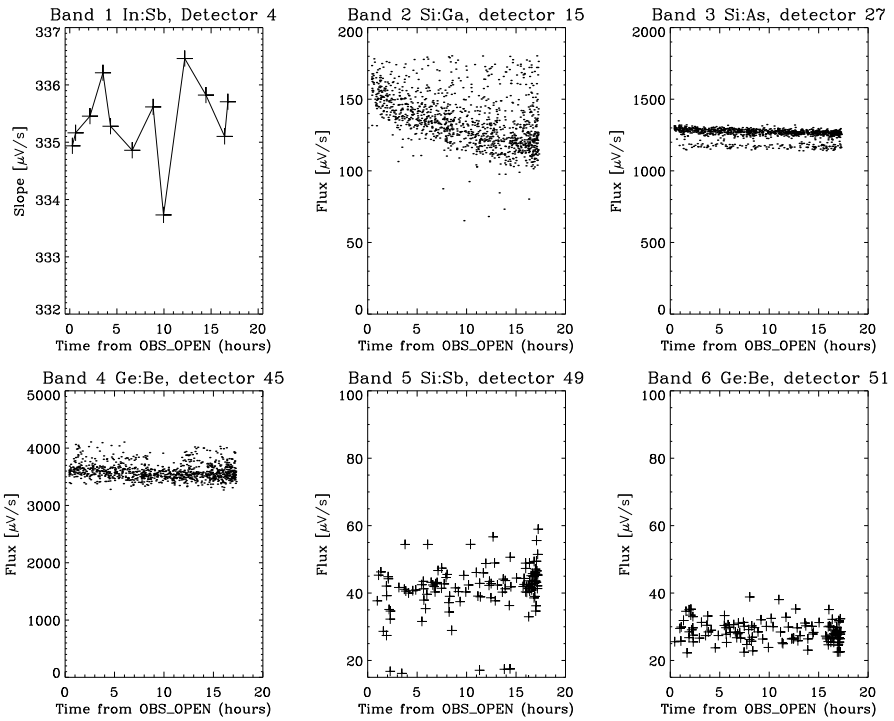

Figure 7. Detector responses as a function of time after the start of the science observation window (or ISO's position in orbit).

calibrator source, set high, were executed at different times along the orbit. This is represented in the first panel of Figure 7, which shows that band 1 is stable within 2%. The stability of the InSb detectors has been also reported by Moseley *et al.* (1989), in relation with the testing of the DIRBE instrument on board the COBE satellite.

3. Effects of the radiation environment

It is well known that space radiation produces a number of undesirable effects in infrared detectors, like signal glitches, noise increase or variations in responsivity (e.g. Kalma, 1980; Young *et al.*, 1989; Price *et al.*, 1992; Patrashin *et al.*, 1995). The space radiation environment of ISO consisted of protons and electrons trapped in the Earth's radiation belts, high energy galactic cosmic rays and solar cosmic rays. The trapped proton belts contain protons with energies up to several hundred MeV and extend to a geocentric distance of four R_E. A few millimeters of aluminium are typically used to shield the detectors from direct exposure to charged particles. However, the most energetic of

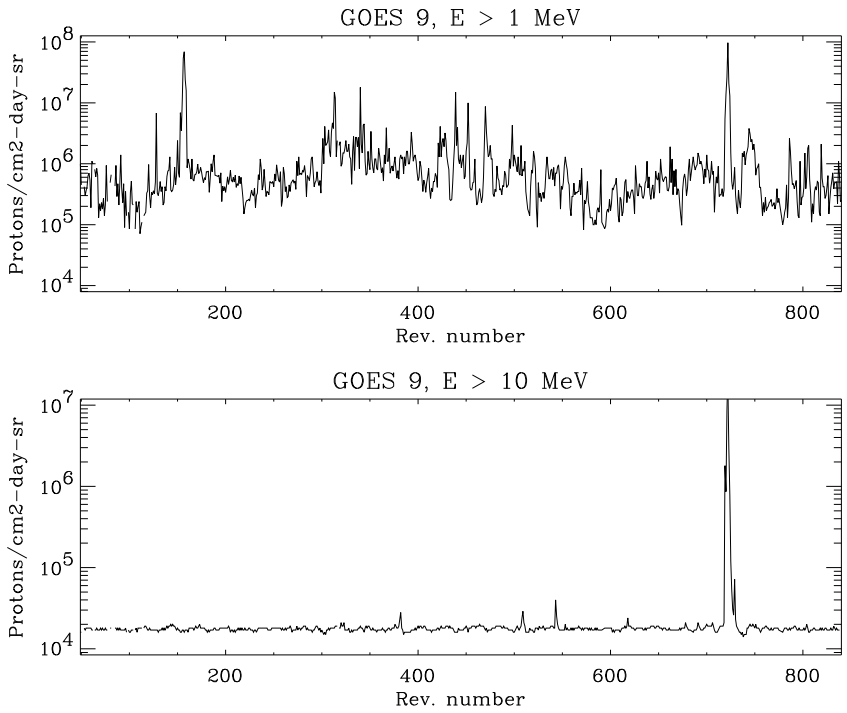

Figure 8. Daily proton fluence measured on the GOES 9 satellite (Space Environment Center, NOAA) during the ISO mission.

these particles may still be able to penetrate the shielding, as well as inducing the production of secondary radiation (e.g., Bremsstrahlung photons caused by the slowing down of charged particles in materials, which is especially important for electrons). Therefore, in order to avoid damage to the detectors and electronic components caused by trapped protons, the ISO instruments were routinely switched off around perigee passage. The trapped electron belts are formed by energetic electrons of energies up to a few MeVs, that extend to a geocentric distance of 10 R_E, that is, covering most of ISO's orbit. The electron environment is very dynamic with fluxes varying diurnally, and as a result of storms and injection events. With regard to solar particle events, ISO was in the favourable situation of operating around the minimum of the solar cycle. This meant that it was not affected by intense solar proton events, except for the large event on November 6, 1997. Figure 8 displays the quiet proton environment during ISO's lifetime as measured on GOES 9 (Space Environment Center, NOAA), with the only important flux increase on November 4-6, 1997 (revolutions 720-722) and a soft event in April 1996 (revolution 152).

Table II. Minimum and maximum voltage jumps detectable in SWS glitches

Gain	Minimum voltage (mV)	Maximum voltage (mV)
Gain 1x	0.1	88
Gain 4x	0.027	22
Gain 16x	0.007	5

3.1. Data

A particle hitting a detector deposits a certain amount of energy so that it induces a jump in the voltages measured during a time reset interval, that is, it causes a glitch in the ramp. The statistical study presented here is based on glitches as identified by the SWS Off-line Processing algorithms (Wieprecht *et al.*, this volume). When calculating glitch rates, it is important to take into account that the detectability of a glitch depends on the slope of the ramp where it occurs. The glitch height in ramps with pronounced slopes must be greater than in flat ramps in order to be detectable. In the same way, the gain setting influences the glitch recognition. Applying a certain gain to a ramp implies multiplying the glitch height by the corresponding gain factor. This amplification ensures that a glitch that would be confused with the ramp noise, stands out after applying a higher gain. As a consequence, observations with low gain have associated lower glitch rates. For consistency, we have restricted our study to observations in which the gain was set to the maximum value, 16x. However, it should be kept in mind that the instrument design, the noise of the ramp measurement and the glitch recognition software set the minimum and maximum glitch height that can be detected (see Table II).

The observations selected for this study are: (1) Observations in calibration revolutions (once a week) just after the science window started; (2) observations in calibration revolutions executed around apogee passage; (3) daily measurements at the end of the activation sequence ($\approx$ 3 hours after perigee passage); and (4) daily observations at apogee.

3.2. Results

3.2.1. *Glitch Rates*

Table III displays the average glitch rates for each detector band, calculated for observations with gain 16x. As can be seen, the most affected detectors are the Ge:Be ones, with glitch rates almost one

order of magnitude higher than in the other bands. In bands 1 and 3 the determination of the glitch rate per unit area is difficult due to the very small z-dimensions of the detectors, which are not precisely known. It must be pointed out that there are two main factors that influence the glitch rate calculation. First, the first six samples in a ramp are discarded in the data processing to avoid the after-reset-pulse effect. Taking this into account would increase the derived glitch rates by $\approx$ 15%, depending on the reset time interval. Second, due to residual cross-talk in the detector arrays, one particle hit may be counted as several glitches, an effect that is particularly significant in band 6 (Ge:Be). A glitch temporal analysis in this band shows that the calculated glitch rate is overestimated with respect to particle hits by $\approx$25%. Considering the net contribution of both factors, the actual particle impact rate in band 6, for example, would be $\approx$10% lower than the glitch rate displayed in Table III. It is important to note that the glitch rates per unit area (third column) are between 2 and 4 times higher than the value of 4 particles/cm^2/s for the cosmic ray flux, predicted by the CREME96 model (Tylka *et al.*, 1997; Nieminen and Sorensen, this volume).

In Figures 9 and 10, the glitch rates for bands 2, 4, 5 and 6 are plotted as a function of ISO revolution number. In the bottom panels the electron fluxes with E $>$ 0.6 MeV and E $>$ 2 MeV measured by GOES 9 are shown. Note that there are no electron data for the November 6, 1997 event in the GOES 9 satellite due to saturation. As can be seen, there is a clear correlation, both in the long and short term features, between the glitch rates in bands 4, 5, and 6 and the electron flux, for the observations carried out close to perigee (when ISO and GOES 9 were at similar altitudes, $\approx$ 4.5 R_E). In the other bands, the glitch rate was not high enough for the correlation to appear clearly, because of the smaller detector areas. No correlation with the GOES 9 electron flux measurements is seen for observations executed around apogee passage, probably due to the different electron environment in that region (unfortunately we do not have electron flux measurements there). We can therefore conclude that the Ge:Be and the Si:Sb detectors are rather sensitive to electron impacts, which is clearly seen when the satellite crosses the electron belts in high flux regions. In addition to the electron flux contribution, the glitch rate modulation seen in bands 4, 5 and 6 may be also related to the position of the ISO orbit with respect to the magnetosphere. Particularly, in revolutions 215 and 645, when the glitch rates show lower values, the orbit apogee was located at 180 degrees from the Sun-Earth line. In revolution 430, on the contrary, the ISO apogee was located between the Sun and the

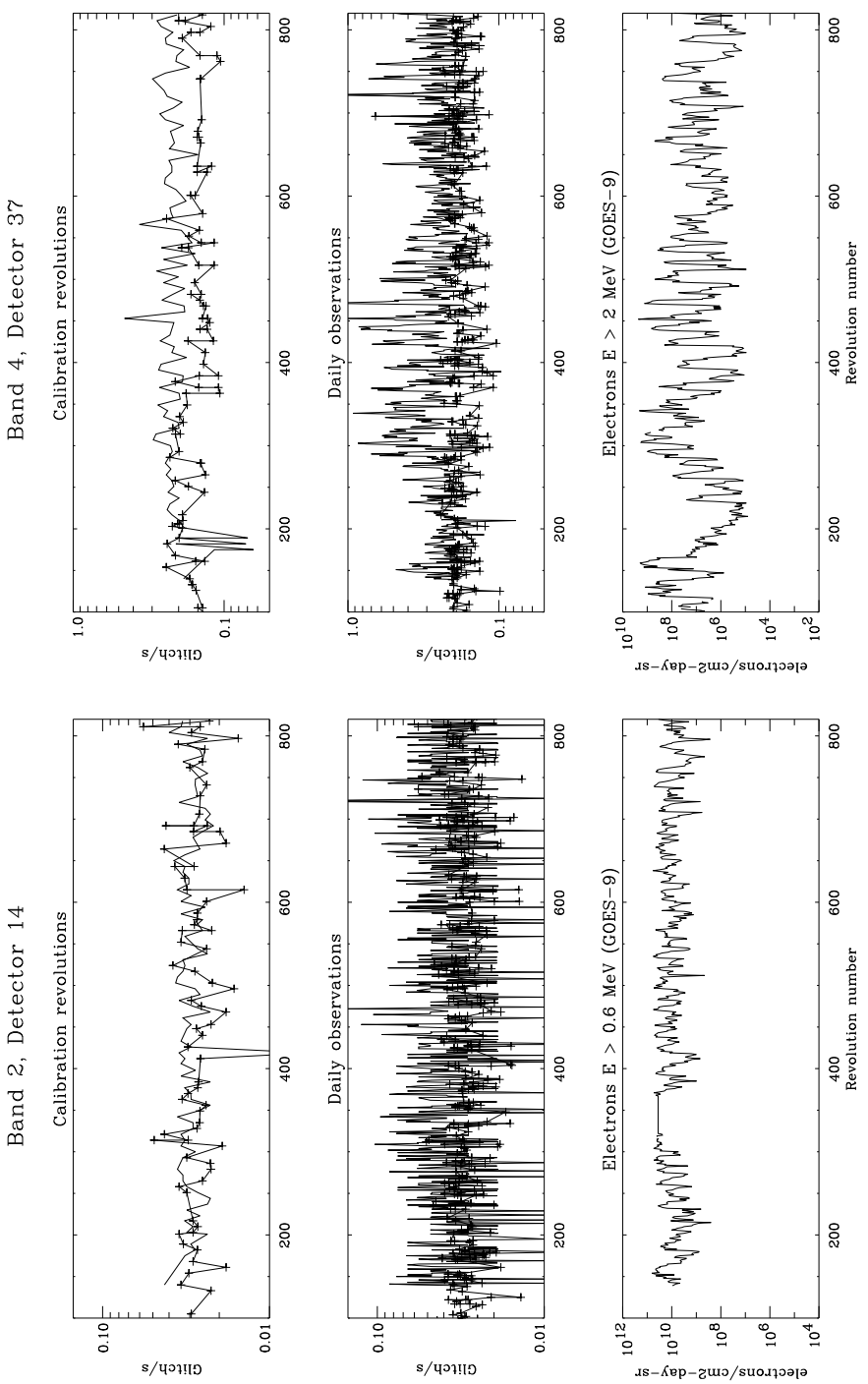

Figure 9. Top panels: Glitch rate as a function of ISO revolution number calculated from observations in calibration revolutions close to perigee (solid line) and close to apogee (line with crosses). Middle panels: Glitch rate as a function of ISO revolution number calculated from daily measurements during the SWS activation sequence, close to perigee (solid line) and from observations executed close to apogee (line with crosses). Bottom panels: Electron daily fluence measured by GOES 9, for E > 0.6 MeV (left) and E > 2 MeV (right).

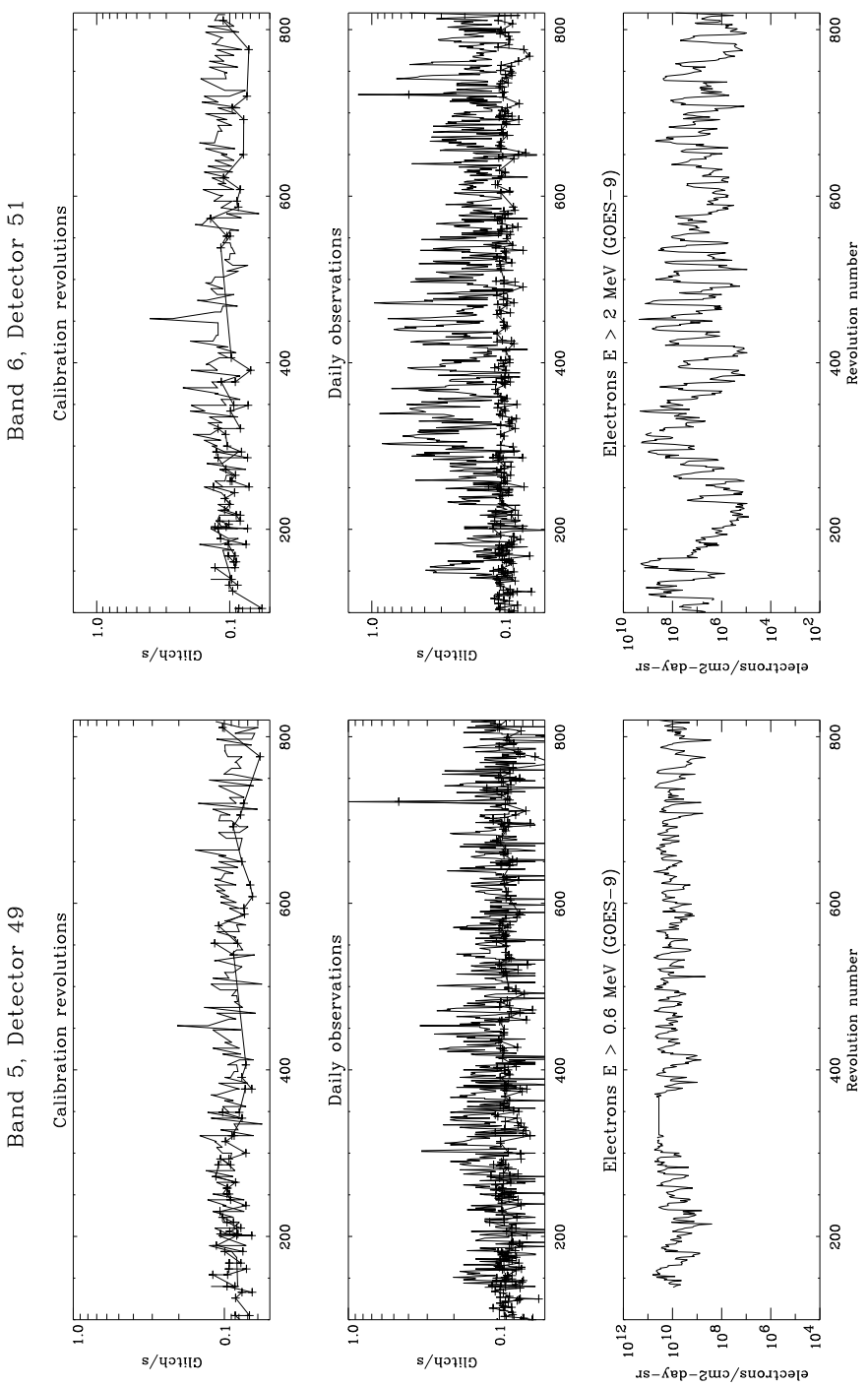

Figure 10. The same as Figure 9 for bands 5 and 6.

Table III. Glitch rates per detector

Detector band	Glitch rate (gain 16x) (s^{-1})	Glitch rate (cm^{-2} s^{-1})
Band 1, InSb	0.005 ± 0.002	-
Band 2, Si:Ga	0.025 ± 0.005	10.0
Band 3, Si:As	0.015 ± 0.007	< 22
Band 4, Ge:Be	0.18 ± 0.05	17.8
Band 5, Si:Sb	0.09 ± 0.02	10.1
Band 6, Ge:Be	0.11 ± 0.03	10.1

Earth on the Sun-Earth line, such that the satellite might have been out of the magnetosphere and therefore more vulnerable to solar particles.

3.2.2. *The November 6, 1997 event*
The increase of the proton flux at energies greater than 10 MeV and 100 MeV measured on the GOES 9 satellite, started at 06/1305 UT and 06/1245 UT, respectively. As mentioned above, this is the most intense event to have occurred during the ISO mission. The proton flux was almost three orders of magnitude higher than average for protons with E > 10 MeV and more than one order of magnitude higher for protons with E > 100 MeV. Moreover, an interplanetary shock arrival and a Sudden Storm Commencement took place at 06/2252 UT, caused by a solar event on the 4th. Figure 11 shows, for bands 1 to 4, dark currents, dark noise, grating calibrator, set low, response and glitch rates measured during the days surrounding the event. The dramatic increases of these parameters caused by the particle event, affected the ISO observations such that they were all declared failed. Castañeda and Klaas (this volume) and Claret *et al.* (this volume) describe the effects of the solar particle event on the ISOPHOT and ISOCAM instruments, respectively. Actually the most affected SWS observation was the first one in the revolution, at the time when the proton flux was at its maximum. Therefore it appears that the proton flux originating in the solar flare on the 6th was primarily responsible for the observed effects on the detectors, and that the "Sudden Storm Commencement" which started three and a half hours after the first observation, and which was associated with the November 4th event, was less significant. An increase in the dark current level was observed in all detector bands, except for band 2, ranging from 25% in band 3 to almost 200% in bands 1 and 4. The dark current noise increased about 200% in all bands. Concerning the responsivity, it was reduced during the proton

event, by 30%, 10% and 15% in bands 2, 3, and 4, respectively. The change in responsivity in band 1 cannot be assessed because it was not monitored during the observations. The glitch rate reached values between five and ten times the nominal rate in all bands, decreasing with time after its maximum during the first observation. All detector parameters were back to normal in the following revolution, although the flux of protons with E > 10 MeV had only decreased by half an order of magnitude. A possible reason is that the detector behaviour was only affected by high fluxes (> 100 protons/cm^2-s-sr) of protons with E > 30 MeV, or mainly by the higher energy protons (E > 100 MeV). This is consistent with the fact that low energy protons could not penetrate the shield, as expected from the shielding model for ISO (Metcalfe and Kessler, 1991). It may also indicate that the contribution to the glitch rate from electron injection events taking place during the intense geomagnetic disturbances was significant.

3.2.3. *Glitch height analysis*

The glitch height is directly related to the energy deposited by the particles that hit the detector. Knowing the detector material characteristics, it is possible to derive information about the incident particles. For this purpose we have calculated the distribution of glitches as a function of the glitch height, deriving from the glitch voltage jump the energy deposited by the incident particle (see Metcalfe and Kessler 1991, appendix C, for a detailed explanation of the method followed). In order to avoid having a biased distribution due to the dependence of the glitch recognition on the flux (i.e., the slope of the ramp), we have set the upper limits to the flux for bands 1, 3 and 4 as 2.5 x 10^3 μV/s, 2.5 x 10^4 μV/s and 1.0 x 10^4 μV/s, respectively. For lower fluxes the dependence of the glitch height on the flux is negligible. The results are displayed in Figure 12, where the thin line corresponds to measurements carried out just before the opening of the science window, the thick line to observations executed at apogee and the dotted line to observations in revolution 722, during the 1997 November event. For comparison, the average energy deposited by a secondary electron, emitted on absorption of a Bremsstrahlung photon produced after the absorption in the satellite material of a trapped electron is about 0.1-0.2 MeV in the Si detectors and $\approx$ 0.1 MeV in the Ge:Be detectors (derived from Metcalfe and Kessler, 1991; Petroff, 1978). In the case of cosmic ray protons, the average deposited energy is 0.1-0.2 MeV in the Si and $\approx$0.3 MeV in the Ge detectors (assuming an average energy deposited of 0.4 MeV/mm in Si and 0.72 MeV/mm in Ge). A model shield, in which the detector is at the center of a sphere composed of 15 mm of aluminium, followed by 2 mm of lead and finally by another

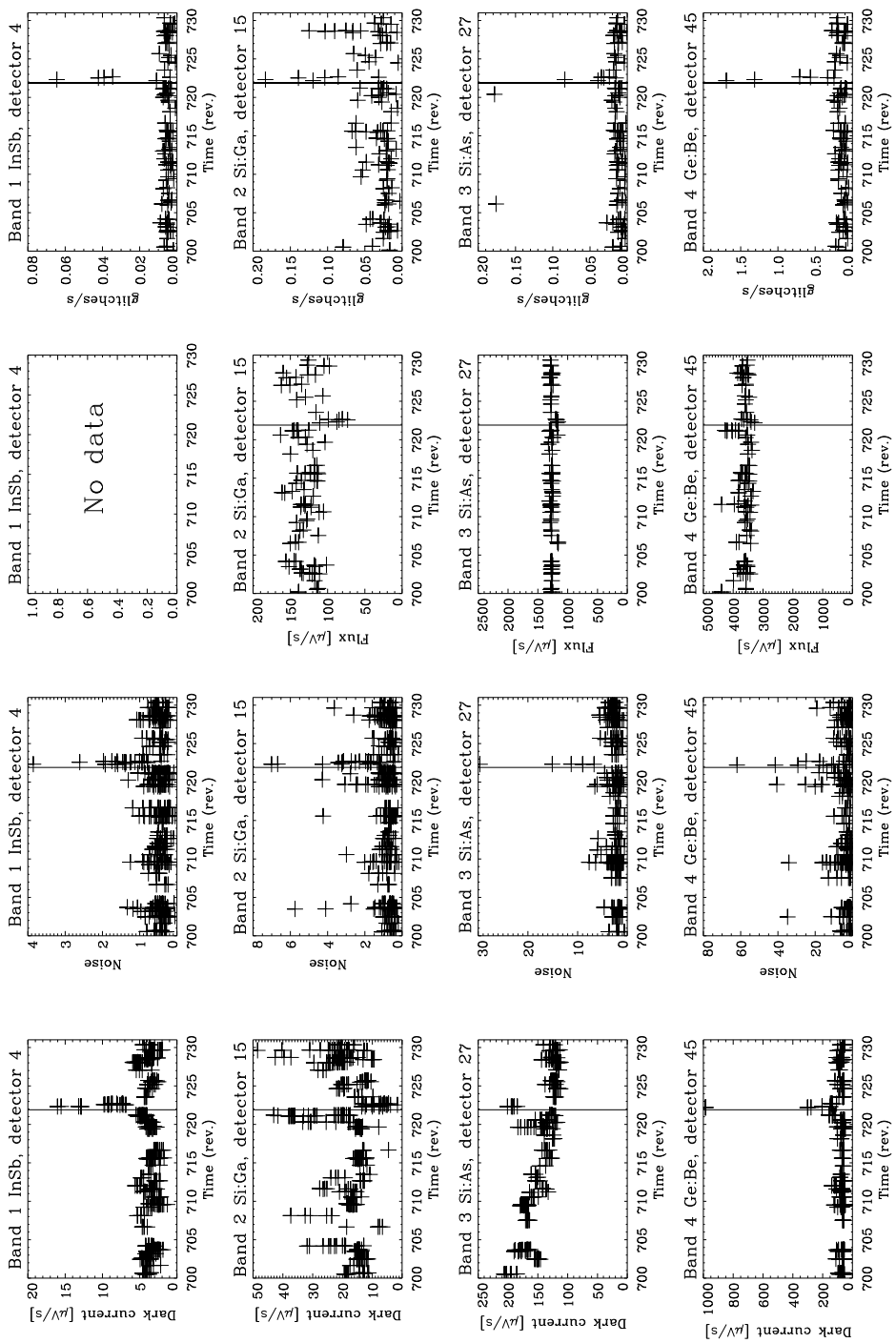

Figure 11. Dark currents, dark current noise, detector response to the grating calibrator source, set low, and glitch rate during the November 6, 1997 event.

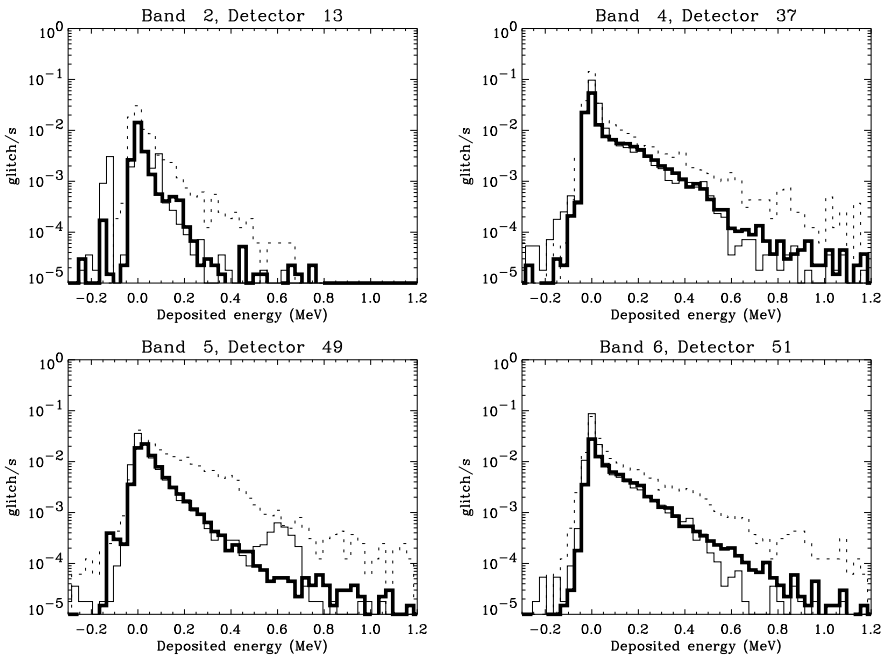

Figure 12. Energy deposited distribution of the impacts rate in observations executed at apogee (thick solid line), measurements just before the opening of the science observation window (thin solid line) and during the November 6, 1997 event in revolution 722 (dashed line).

2 mm of aluminium, has been assumed both for the electron and the proton calculations. Figure 12 shows that the distribution maximum in all bands corresponds to a deposited energy of ≈0.01 MeV, being the minimum detectable deposited energy 1 keV. Taking into account that 55% of the glitches in band 4 have associated a deposited energy lower than 0.07 MeV, it can be concluded that more than half of the impacts are related to secondary electrons (and other secondary particles) and the rest to cosmic rays. In Si detectors the contribution from electrons and protons is more difficult to disentangle. Nevertheless, secondary particles produced in the detectors and the shield can also explain the difference mentioned above, between the observed glitch rates in these bands and the predicted value for the cosmic ray flux (a factor 2 to 4 lower). As shown in Figure 12, the similarity between the close to perigee and at apogee distributions is remarkable, indicating that the nature of the particles associated with the glitches is the same. During the November 6, 1997 big proton event, the glitch height distribution became harder in all bands, indicating a larger contribution from high

energy proton impacts. However, the maximum of the distributions was still at the lowest deposited energies, showing the large contribution from secondary particles to the glitch rate increase.

4. Conclusions

We have studied the ISO-SWS detectors performance trends as a function of time through the mission and as a function of time in a revolution. Dark currents, dark current noise and detector responses were stable as a function of time in all bands but for band 3 (Si:As), in which the dark currents, and in some detectors also the noise, increased during the mission. Dark currents in the first four hours after the start of the science window were higher in all bands, this effect being more important for bands 2, 4 and 6. Detector responses were also found to be higher especially in band 2. On the contrary, there was no variation of the noise level in any band along the revolution.

The space radiation environment of ISO was dominated by galactic cosmic rays and trapped electrons and protons. Only one intense solar proton event occurred during the ISO mission, since the satellite was operated during solar minimum. Bands 4, 6 (Ge:Be) and 5 (Si:Sb) registered the highest glitch rates, which showed a correlation with the electron fluxes measured on GOES 9 for observations executed close to perigee. This fact, the observed glitch rates being higher than the predicted value for the cosmic ray flux, and the analysis of the glitch height distributions, support the conclusion that secondary particles contributed at least as much as cosmic rays to the glitch rates in the SWS detectors.

References

Castañeda, H., Klaas, U.: "Space weather impact on the ISOPHOT detectors", this volume

Claret, A., Dzitko, H., Engelmann, J., Starck, J.-L.: "Glitch effects in ISOCAM detectors", this volume

de Graauw, Th. et al.: 1996, "Observing with the ISO Short-Wavelength Spectrometer", *A&A*, **Vol. 315**, pp. L49-L54

Kalma, A.H.: 1980, "Nuclear and space radiation effects in infrared detectors", *SPIE Proc.*, **Vol. 217**, pp. 186-191

Metcalfe, L., Kessler, M.F.: *Scientific Capabilities of the ISO Payload*, ISO-SSD-8805, issue 1.0, 1991.

Moseley, S.H., Silverberg, R.F., Lakew, B.: 1989, "Effects of ionizing radiation on cryogenic infrared detectors", *SPIE Proc.*, **Vol. 973**, pp. 299-307

Nieminen, P., Sorensen, J.: "ISOCAM LW detector glitches: Data and ray-tracing simulations", this volume

Patrashin, M.A., Fouks, B.I.., Lemke, D., Wolf, J.: 1995, "Radiation-induced effects in extrinsic far-infrared detectors",*SPIE Proc.*, **Vol. 2475**, pp. 476-486

Petroff, M.: "Effect of natural radiation environment on the IRAS IR detectors", *IRAS eng. lett. report*, 1978.

Price, M.C., Griffin, M.J., Church, S.E., Murray, A.G., Ade, P.A.R.: 1992, "Ionising radiation-induced effects in doped germanium FIR photoconductors", *Proceedings of an ESA Symposium on Photon Detectors for Space Instrumentation*, pp. 309-312

Tylka, A.J., et al.: 1997, "CREME96: A revision of the cosmic ray effects on microelectronics code", *IEEE Transactions on Nuclear Science*, **Vol. 44**, p. 2150

Wieprecht, E., Haser, L. and Wiezorrek, E.: "SWS–Detector glitch effect correction", this volume

Young, E.T., Rieke, G.H., Low, F.J., Haller, E.E., Beeman, J.W.: 1989, "Ga:Ge array development", *Proceedings of the Third Infrared Detector Technology Workshop*, pp. 125-133